28p.

N62-16855

NASA TN D-1425

TECHNICAL NOTE

D-1425

FREE-FLIGHT TESTS OF FIFTH-STAGE SCOUT ENTRY VEHICLE AT MACH NUMBERS OF 5 AND 17

By Donn B. Kirk and Robert J. Miller

Ames Research Center
Moffett Field, Calif.

NATIONAL AERONAUTICS AND SPACE ADMINISTRATION

WASHINGTON October 1962

NATIONAL AERONAUTICS AND SPACE ADMINISTRATION

TECHNICAL NOTE D-1425

FREE-FLIGHT TESTS OF FIFTH-STAGE SCOUT ENTRY VEHICLE AT MACH NUMBERS OF 5 AND 17

By Donn B. Kirk and Robert J. Miller

SUMMARY

Measurements have been made in air at two Mach numbers of the static stability, normal force, and drag of a version of the fifth-stage Scout entry vehicle. The most significant result was that the design center of gravity led to a condition of static instability at small angles of attack at Mach number 17. At this Mach number, the static stability was a highly nonlinear function of the angle of attack. A useful method for analyzing free-flight data having this nonlinear behavior is included in this report.

Comparisons were made between the measured aerodynamic coefficients and those estimated by Newtonian impact theory and by a method developed by Seiff and Whiting. The latter method gave good estimates of the normal-force-curve slope at both Mach numbers and of the moment-curve slope at the lower Mach number. It resulted in an overestimation of the static stability at Mach number 17, although it gave results decidedly closer to the experimental value than did Newtonian impact theory.

INTRODUCTION

The Scout configuration considered in this report is an early version of the fifth and final stage of a research vehicle designed to study aerodynamic heating problems in atmosphere entry. In operation, the first two stages are fired to lift the vehicle out of the measurable atmosphere. The vehicle is then directed downward, and the three remaining stages accelerate it into the atmosphere to a peak velocity of about 30,000 ft/sec. Thus, the vehicle under consideration includes a rocket motor, heat shield, and instrumentation associated with the experiment.

About a year ago, testing of the fifth stage of the Scout configuration was initiated in the Ames free-flight facilities. Of primary interest was the static stability at the highest Mach number attainable. Small-scale models having centers of gravity positioned at the design center of gravity were constructed and three firings were made - two at Mach number 14 and one at Mach number 5. The test at Mach number 5 yielded data that compared favorably with wind-tunnel tests and indicated that the model was both statically and dynamically stable. The tests at Mach number 14, however, resulted in motions that gave evidence of static

instability at angles of attack up to about 6°. These motions were such that only qualitative statements concerning the stability could be made.

To define the stability of this configuration at high Mach numbers with more precision, another group of models was made with the center of gravity located farther forward. Seven tests were made of these models at a Mach number of about 17. In this case, it was possible to obtain a quantitative estimate of the static stability over a wide range of amplitudes. In addition, measurements were made of the normal-force-curve slope and drag of the test configuration. A complete description of this investigation will be given in this report, together with a comparison of the experimental data and that predicted by Newtonian impact theory and by a recent theoretical method (refs. 1 and 2).

SYMBOLS

C_D drag coefficient, $\frac{\text{drag}}{qS}$

C_{L_α} lift-curve slope, $\frac{dC_L}{d\alpha}$

C_m restoring-moment coefficient, referred to model center of gravity, $\frac{\text{restoring moment}}{qSd}$

$C_{m_q} + C_{m_{\dot{\alpha}}}$ damping-in-pitch derivative

C_{m_α} moment-curve slope, $\frac{dC_m}{d\alpha}$

$C_{m_{\sigma_L}}$ moment-curve slope obtained from linear theory, $\frac{-8\pi^2 I}{57.3\lambda^2 \rho S d}$, per deg

C_{N_α} normal-force-curve slope, $\frac{dC_N}{d\alpha}$, per deg

d reference length, maximum diameter of model

I moment of inertia about an axis through the center of gravity of the model and normal to the axis of symmetry

m mass of model

M free-stream Mach number

q free-stream dynamic pressure, $\frac{\rho V^2}{2}$

R	Reynolds number, $\frac{\rho V d}{\mu}$
S	reference area, $\frac{\pi d^2}{4}$
V	model velocity relative to airstream
x	distance along the trajectory
x_{cg}	center-of-gravity location measured from nose
x_{cp}	center-of-pressure location measured from nose
α	angle of attack
β	angle of sideslip
λ	wave length of pitching oscillation relative to airstream
μ	coefficient of viscosity in free stream
ρ	density of undisturbed airstream
σ	resultant angle of attack, measured between model center line and airstream ($\tan^2\sigma = \tan^2\alpha + \tan^2\beta$)
σ_m	maximum resultant angle of attack attained during a given flight
σ_o	minimum resultant angle of attack attained during a given flight
$\sqrt{\overline{\sigma^2}}$	root-mean-square resultant angle of attack for a given flight

Subscript

i	value at $\alpha = 0^\circ$

DESCRIPTION OF TESTS

A series of tests of the fifth-stage Scout entry vehicle was conducted in the Ames Supersonic Free-Flight Wind Tunnel (ref. 3) and in the Ames Pressurized Ballistic Range. The conditions of the tests can be summarized as follows:

Model center of gravity	No. fired	Launched into	Facility	M	R
Design	1	Still air at 0.16 atm pressure	PBR	5	0.2×10^6
Design	2	M = 3 airstream	SSFF WT	14	3.5×10^6
Forward	7	M = 3 airstream	SSFF WT	17	$2\text{-}4\times10^6$

Three different smooth-bore guns were used to launch the models into flight: for the Mach number 5 tests, a caliber 50 powder-gas gun, and for the other tests, single-stage shock-compression light-gas guns with launch-tube bore diameters of 0.5 inch and 37 mm.

Models and Sabots

The models and sabots used are shown in figures 1 and 2. The model shown in figures 1(a) and 2(a), used in the tests at Mach numbers of 5 and 14, was a scale model of one version of the fifth-stage Scout entry vehicle. The center of gravity was located to correspond to that of the full-scale vehicle with its rocket fuel expended.

The tests at Mach number 17 required a model with a more forward center of gravity. To assist in shifting the center of gravity and, in addition, make the models easier to build, the rocket exhaust fairing on the model base was eliminated. This fairing was assumed to have a negligible effect on the static stability. These models are shown in figures 1(b) and 2(b).

Both types of models were made of aluminum alloy with tungsten alloy nose ballasts used to adjust the location of the center of gravity. Physical characteristics of all models tested are listed in table I.

Two-piece split sabots illustrated in figure 2 were used to launch the models. For the 0.50-inch guns, sabots were made of Lexan polycarbonate plastic. A novel technique was used in forming the front of the sabot to insure a precise fit to the contoured rear face of the model; the model was simply heated and pressed into the sabot. For the 37-mm gun, sabots of ethyl cellulose plastic were used, with a hemispherical aluminum load-bearing insert under the model. All sabots featured pins running across the parting plane to prevent shearing motion between halves while moving down the gun. The 0.50-inch-diameter sabots were separated by gun gas trapped in the hole drilled forward along the axis of the sabot, while the 37-mm sabots were separated by aerodynamic forces acting on a forward-facing bevel around the periphery.

Figure 3 shows typical shadowgraphs taken in these tests - one each at Mach numbers of 5 and 17. In both shadowgraphs the models are near 0° angle of attack.

STATIC-STABILITY DATA REDUCTION

A number of distinct types of model motions encountered during this series of tests led to the use of different methods of data reduction for obtaining the static stability. Three representative motions are shown in figure 4. Figure 4(a) shows the model motion during the Mach number 5 test, which was conducted in the Ames Pressurized Ballistic Range at a pressure of 0.16 atmosphere. Because of this low pressure, the Mach number remained essentially constant over the entire trajectory (130 ft). As an attempt in fitting this data, a method developed by Nicolaides (ref. 4) was used. This method is based on the assumption of a linear restoring moment. It can be seen from a comparison of the fitted theoretical motion history with the observed data points in this figure that the method gave a good fit to the experimental data. The fact that it worked over such a long trajectory gives support to the validity of the method.

Figure 4(b) shows the motion encountered in one of the tests at Mach number 14. This motion was characterized by a large apparent trim angle and by a tendency of the resultant angle of attack trace to swerve away from the origin of coordinates. Both of these characteristics suggested that the model was unstable at small angles of attack, but became stable at some higher angle. No method was found that could yield quantitative measurements of the static stability from these tests; hence, the center of gravity of the model was moved forward and additional high Mach number tests were conducted.

The tests of the model with the forward center of gravity were conducted at a Mach number of about 17. Figure 4(c) shows the motion obtained from one of these tests. All of these motions were characterized by relatively narrow ellipses in the α - β plane. This series of tests resulted in peak oscillation amplitudes ranging between a low of 10-1/2° and a high of 40°. It was found that the wave length of the model oscillation was dependent on the amplitude (see table I). This indicated that the restoring moment was nonlinear with angle of attack and required an appropriate method of nonlinear analysis. Several suitable methods of analysis have been devised, including those of Rasmussen (ref. 5) and Murphy (ref. 6). The method used to analyze these tests was that of Rasmussen.

Figure 5 shows the experimental data from the series of tests at Mach number 17 plotted in a manner suggested by Rasmussen. The ordinate is the moment-curve slope obtained with the assumption that a <u>linear</u> restoring moment governs the model $\left(C_{m_{\sigma_L}} = \frac{-8\pi^2 I}{57.3\lambda^2 \rho S d}\right)$; the abscissa is the sum of the squares of the maximum and minimum resultant angles of

attack. Each data point represents the firing of a single model. Rasmussen's analysis indicates that this plot will result in a straight line if a moment of the form $C_m = A\sigma + B\sigma^3$ governs the model. It is apparent from this figure that no single straight line can be drawn through all the data points. However, it is seen that a straight line is a good representation of the data in the high angle region, thus establishing the restoring moment in this region. The question as to what the moment is in the low angle region is more complicated.

To answer this question, one of the low amplitude runs (957) was chosen for detailed analysis. It was assumed that the restoring moment governing this model throughout its amplitude spectrum (from about 1° to 12°) was of the form $C_m = A\sigma + B\sigma^3$. An attempt was then made to see if values of A and B existed that would lead to a motion, $\sigma(x)$, reasonably close to the observed variation. Equations from reference 5 were used and will be elaborated later. The results of this analysis are shown in figure 6(a). It is seen that an excellent representation of the motion was obtained with a restoring moment of the assumed form. Included for comparison purposes is the motion that would result from the assumption of a linear moment; in this case, the data points deviate from the theoretical motion history in a systematic way. It should be emphasized here that the use of a linear plus cubic moment does not guarantee a good fit of the experimental data. Although a more complicated nonlinear moment could undoubtedly lead to a better fit, the excellent fit obtained with the linear plus cubic moment in the present case makes a strong argument for this being a valid approximation to the true restoring moment.

This argument is made even stronger in figure 6(b). Here the experimental data points from the second low amplitude run (962) are shown together with the theoretical representation of the motion obtained with the restoring moment found from run 957. Once again the agreement is excellent, and again much superior to the motion resulting from the assumption of a linear moment. The straight line corresponding to this low amplitude cubic-moment curve is indicated in figure 5.

The way in which the coefficients of the linear and cubic terms of the restoring moment were found can be explained briefly as follows. In reference 5, the restoring-moment coefficient is assumed to be

$$C_m = -\frac{2I}{\rho S d}\left(M_0\sigma + 2M_1\sigma^3\right) \tag{1}$$

For the cases where the linear term is either stabilizing or destabilizing and the cubic term is stabilizing, the solution for the resultant angle of attack as a function of distance along the trajectory is found to be

$$\sigma^2 = \frac{\sigma_0^2 - t_3 k_1^2 \operatorname{sn}^2\left[\sqrt{M_1(\sigma_m^2 - t_3)}\,(x - x_0)\right]}{1 - k_1^2 \operatorname{sn}^2\left[\sqrt{M_1(\sigma_m^2 - t_3)}\,(x - x_0)\right]} \tag{2}$$

where

$$t_3 = -\left(\sigma_m^2 + \sigma_o^2 + \frac{M_o}{M_1}\right)$$

$$k_1 = \sqrt{\frac{\sigma_m^2 - \sigma_o^2}{\sigma_m^2 - t_3}} \equiv \text{modulus of complete elliptic integral of the first kind, } K(k_1)$$

$$\sqrt{M_1(\sigma_m^2 - t_3)} = \frac{K(k_1)}{\lambda/4} \qquad (3)$$

sn u $\equiv$ Jacobian elliptic function, sine amplitude u

To find the restoring-moment coefficient from a given run:

1. Assume M_o/M_1
2. Find t_3, k_1, $K(k_1)$, $\sqrt{M_1(\sigma_m^2 - t_3)}$
3. Find $\sigma(x)$ from equation (2)
4. Determine $\sum_{\substack{\text{all} \\ \text{stations}}} (\sigma - \sigma_{exp})^2$, σ_{exp} = experimental value of σ
5. Repeat for other values of M_o/M_1
6. Determine least squares value of M_o/M_1 graphically as follows:

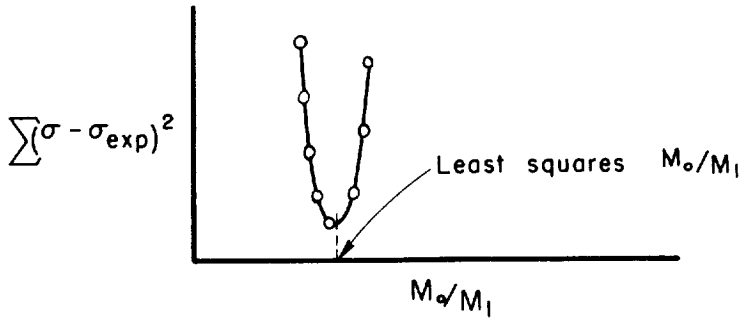

7. Use equation (3) to find M_o and M_1 separately
8. Find the restoring-moment coefficient from equation (1)

Several minor changes are needed to treat the case where the linear term in equation (1) is stabilizing and the cubic term is destabilizing.

For this case, equation (2) becomes

$$\sigma^2 = \sigma_o^2 + (\sigma_m^2 - \sigma_o^2)\ sn^2 \left[\sqrt{M_1(\sigma_o^2 - t_3)}\ (x - x_o) \right] \qquad (2a)$$

and the following expressions are used:

$$t_3 = -\left(\sigma_m^2 + \sigma_o^2 + \frac{M_o}{M_1} \right)$$

$$k_2 = \sqrt{\frac{\sigma_m^2 - \sigma_o^2}{t_3 - \sigma_o^2}}$$

$$\sqrt{M_1(\sigma_o^2 - t_3)} = \frac{K(k_2)}{\lambda/4} \qquad (3a)$$

With these modifications, the procedure is identical.

RESULTS AND DISCUSSION

All the data obtained in this investigation are presented in table I together with the test conditions and pertinent model geometry for each firing. In the following sections, the data are presented graphically and comparisons are made with related data from other experiments and with theory.

Static Stability

The static-stability characteristics obtained by the methods outlined in the preceding section can be summarized here as follows:

Mach number 5 (moments about design center of gravity, $x_{cg}/d = 0.765$)

$$C_{m_{\alpha_i}} = -0.0022 \text{ per degree}$$

Mach number 17 (moments about model center of gravity, $x_{cg}/d = 0.706$)

$$C_m = -0.00036\alpha - 0.000021\alpha^3 \quad 0^\circ \leq \alpha \leq 12^\circ$$

$$C_m = -0.0056\alpha - 0.0000011\alpha^3 \quad 23^\circ \leq \alpha \leq 40^\circ$$

α in degrees

Figure 7(a) shows the restoring moment at Mach number 17 as a function of angle of attack. It is noted from the above equations that the restoring moment remained undefined in the angle-of-attack region between 12° and 23°. However, it is seen in figure 7(a) that the two known segments of the curve are such that a fairing between them defines the restoring moment in this region with little ambiguity.

Figure 7(b) shows a comparison of the low-angle restoring moment of the present report with data from tests in the Langley 11-Inch Hypersonic Tunnel and 22-Inch Helium Tunnel. The wind-tunnel tests were conducted by Mr. Patrick J. Johnston of the Langley Research Center. The model tested in the 22-Inch Helium Tunnel was identical to that of the present tests with the exception that it included the rocket exhaust fairing. The model tested in the 11-Inch Hypersonic Tunnel had several additional modifications. These differences are shown in the following sketch, where scale drawings of the two configurations are superimposed. It is seen that the differences in geometry are small, so that a direct comparison of the data

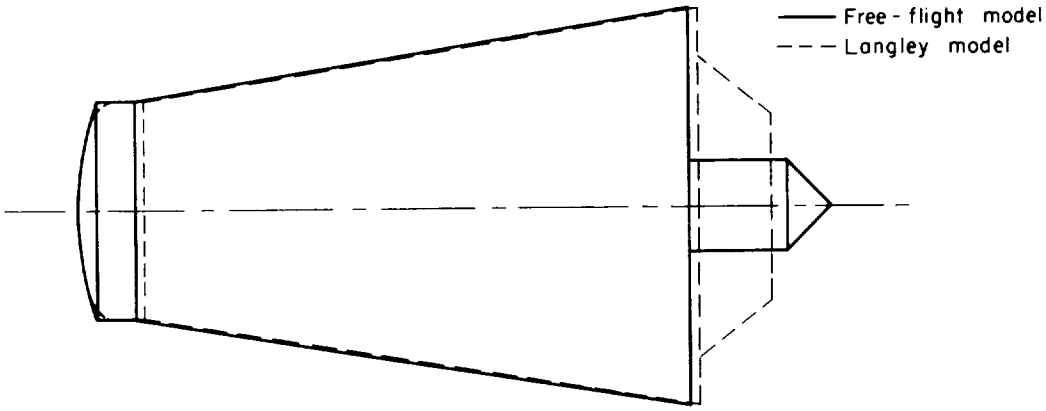

Sketch (b)

is of interest. For this comparison, the Mach number 17 data of the present report have been transferred to the design center of gravity to agree with the moment center used in all the other tests. In making the transfer, the normal-force curve was assumed to be linear with a slope of 0.0125 per

degree. This value is reasonable, as shown later. Figure 7(b) indicates that the results of the present report show trends similar to those of the other facilities. It is to be noted, however, that the helium tunnel indicates stability throughout the angle-of-attack range at Mach number 24, whereas the present tests in air indicate a region of instability in the small angle-of-attack range at Mach number 17.

Dynamic Stability

It was shown in reference 7 that a convenient parameter which describes the dynamic stability of a vehicle flying at constant altitude is of the form

$$\xi = C_D - C_{L_\alpha} + \left(C_{m_q} + C_{m_{\dot{\alpha}}}\right)\left(\frac{md^2}{I}\right)$$

where a negative value of ξ indicates dynamic stability. This parameter was determined from the test conducted at Mach number 5 by use of the tricyclic theory of pitching and yawing motion developed by Nicolaides (ref. 4). The results were as follows:

$$\xi = -0.638$$

$$C_{m_q} + C_{m_{\dot{\alpha}}} = -0.252$$

This indicates that the model was slightly dynamically stable under these conditions.

No dynamic-stability data were obtained for the tests at the higher Mach numbers since fewer than 1-1/2 cycles of model oscillation were observed.

Normal Force and Center of Pressure

To obtain a measure of the normal-force-curve slope, an analysis was made of the oscillations in flight path traced by the centers of gravity of three models - one at Mach number 5 and the two low-amplitude runs at Mach number 17. The results of these analyses, together with data obtained from the Langley Unitary Plan Wind Tunnel and 11-Inch Hypersonic Tunnel, are shown in figure 8(a). Once again it should be noted that the configuration tested in the Langley wind tunnels was not identical to that of the present tests. In this case, the Langley model incorporated a cylindrical section instead of a full flare, as shown in the following sketch.

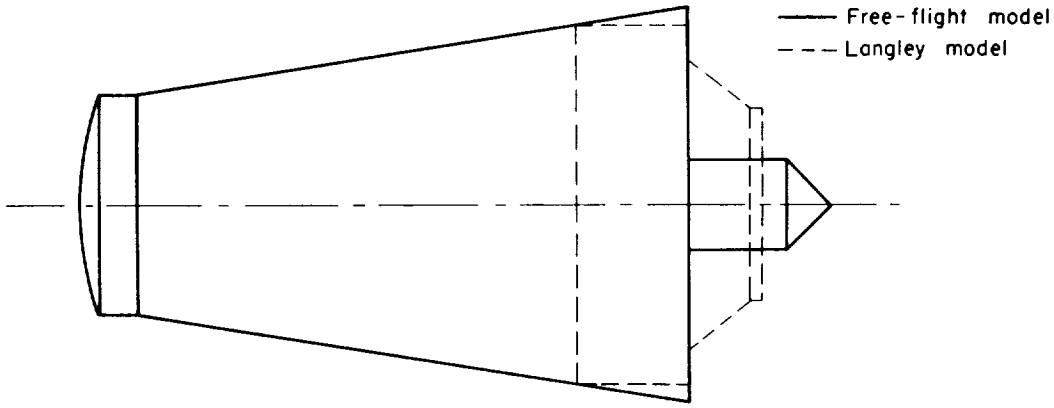

Sketch (c)

This configurational difference would be expected to affect the normal-force-curve slope, but since C_{N_α} in both cases was based on the maximum cross-sectional area of the model tested, the effect should be small. That this is the case is indicated by the close agreement of the present tests with the wind-tunnel data.

To obtain the center of pressure as a function of angle of attack at Mach number 17, it was assumed that the normal-force-curve slope did not depend on angle of attack. An average of the two experimental values obtained (0.0125 per degree) was used for this slope, in conjunction with the experimental restoring-moment coefficient. This led to the curve shown in figure 8(b). This figure indicates that the design center of gravity leads to a configuration that is statically unstable to angles of attack of approximately 4° at Mach number 17, as noted in the discussion of the pitching-moment data. Since it would be expected that the normal-force-curve slope would increase with angle of attack, a more realistic center-of-pressure variation would fall below the curve shown. For this case, static instability would persist to a higher angle of attack than 4°.

Also indicated in this figure is the initial center of pressure obtained from the test at Mach number 5. In this case, it is seen that the configuration is stable with a large static margin.

Comparison With Theory

A comparison was made between the experimentally determined aerodynamic coefficients and those estimated by modified Newtonian theory[1]

[1]Note that modified Newtonian theory replaces the coefficient "2" in the term $C_p = 2 \sin^2\theta$ by the pitot-pressure coefficient.

(ref. 8) and by the theoretical method of Seiff and Whiting (refs. 1 and 2). The results of this comparison are shown in figure 9, where the moment has been referred to the center of gravity of the configuration tested at Mach number 17. It is noted that modified Newtonian theory greatly overestimates the stability at both Mach numbers, and provides a poor estimation of the normal force and center of pressure at a Mach number of 17. The method of Seiff and Whiting provides a significantly better estimation of both the stability and normal force, but still results in an appreciable error in the stability at a Mach number of 17.

That this method works as well as it does should be considered somewhat surprising, since it treats the present configuration as a flare-stabilized blunt-nosed cylinder when it actually deviates very little from a simple truncated cone. Also, the "flare" occurs relatively close behind the blunt nose, a region where the flow-field analysis of reference 1 may tend to become inaccurate. Additional uncertainty at the higher Mach number is attributed to a lack of knowledge concerning the high pressures acting on the short cylindrical section of the model. Because of the large moment arm, this section contributes a relatively large destabilizing moment while contributing little to the normal force.

The method used to obtain these theoretical values can be described briefly as follows: Measurements were first taken from shadowgraphs to find the shape of the bow shock wave. This shock-wave shape was used as an input to the flow-field analysis of reference 1, and the dynamic-pressure field ahead of the secondary shock wave that emanates from the cylinder-"flare" junction was determined. This dynamic-pressure field was used to treat the "flare" according to the method of reference 2, and its contributions to the stability and normal force were obtained from the equations

$$\left(C_{m_{\alpha_i}}\right)_f = 16 \cos^2\theta_f \int \left(\frac{q}{q_\infty}\right)\left(\frac{l}{d}\right)\left(\frac{r}{d}\right) d\left(\frac{r}{d}\right)$$

$$\left(C_{N_{\alpha_i}}\right)_f = 16 \cos^2\theta_f \int \left(\frac{q}{q_\infty}\right)\left(\frac{r}{d}\right) d\left(\frac{r}{d}\right)$$

where

r local body radius

l local moment arm

θ_f flare half-angle

The contribution due to the spherical nose cap was found by means of modified Newtonian theory. Obtaining the moment and normal-force contributions of the cylindrical section first required an estimate of the pressure on this surface at zero angle of attack. This pressure was obtained in two ways. First, it was assumed that the nose-cylinder

junction was slightly rounded, eliminating any discontinuity in slope; the pressure at the front station of the cylinder was then estimated by assuming Prandtl-Meyer expansion through an angle of about 35°, the local body angle at which the slopes of the Newtonian and Prandtl-Meyer pressure distributions coincide. At Mach number 17, this resulted in a pressure ratio relative to free-stream conditions of 29. The other way of estimating this pressure was to use the flow-field analysis of reference 1, although the authors indicated that the analysis becomes less accurate in the region immediately behind the blunt nose. However, at Mach number 17, this resulted in a pressure ratio of 37 relative to free-stream conditions which was considered good agreement. The average of the two results, 33, was used over the entire cylinder. To find the pressure differential between the upper and lower meridians from which the cylinder contributions could be estimated, $\Delta\nu$ was assumed to equal α, as in reference 1. This procedure indicated that at a Mach number of 17 the destabilizing moment attributable to the cylinder was about one-third the magnitude of the stabilizing moment attributable to the "flare."

Drag

Figure 10 shows the drag coefficient as a function of the root-mean-square resultant angle of attack at Mach numbers of 5, 14, and 17. It was shown in reference 9 that this presentation is equivalent to a plot of C_D versus α for a model subjected to static tests if the results are of the form $C_D = C_{D_o} + k\overline{\sigma^2}$. A quadratic of this form is shown in the figure for the Mach number 17 data and is seen to represent the data adequately. Surprisingly, in this figure the Mach number 14 data fall below the Mach number 17 data. The only explanation for this result would appear to be the existence of different amounts of base drag that result from the different base geometries of the models.

CONCLUDING REMARKS

The results of a series of free-flight tests of the fifth-stage Scout entry vehicle can be summarized as follows:

The static stability of the test configuration was strongly dependent on Mach number, becoming less stable as the Mach number increased. The proposed design center of gravity led to a configuration that was statically unstable at small angles of attack at Mach number 17. It was found that increasing the Mach number had the effect of decreasing the initial normal-force-curve slope and moving the center of pressure forward. The restoring moment governing the test configuration at Mach number 17 was found to be a nonlinear function of the angle of attack. A useful method of analyzing this nonlinear behavior was described.

Comparisons were made with results from other facilities; in most cases, the results from the present investigation were found to show reasonable agreement. Comparisons were also made between the experimental data and that estimated by Newtonian impact theory and by the Seiff and Whiting method. This latter method was found to provide a good estimate of all the aerodynamic coefficients at Mach number 5 and of the initial normal-force-curve slope at Mach number 17. Newtonian impact theory was found to provide a relatively poor estimation.

Ames Research Center
National Aeronautics and Space Administration
Moffett Field, Calif., May 25, 1962

REFERENCES

1. Seiff, Alvin, and Whiting, Ellis E.: Calculation of Flow Fields From Bow-Wave Profiles for the Downstream Region of Blunt-Nosed Circular Cylinders in Axial Hypersonic Flight. NASA TN D-1147, 1961.

2. Seiff, Alvin: Secondary Flow Fields Embedded in Hypersonic Shock Layers. NASA TN D-1304, 1962.

3. Seiff, Alvin: A Free-Flight Wind Tunnel for Aerodynamic Testing at Hypersonic Speeds. NACA Rep. 1222, 1955.

4. Nicolaides, John D.: On the Free Flight Motion of Missiles Having Slight Configurational Asymmetries. B.R.L. Rep. 858, Aberdeen Proving Ground, Md., 1953.

5. Rasmussen, Maurice L.: Determination of Nonlinear Pitching-Moment Characteristics of Axially Symmetric Models From Free-Flight Data. NASA TN D-144, 1960.

6. Murphy, Charles H.: The Effect of Strongly Nonlinear Static Moment on the Combined Pitching and Yawing Motion of a Symmetric Missile. B.R.L. Rep. 1114, Aberdeen Proving Ground, Md., 1960.

7. Seiff, Alvin, Sommer, Simon C., and Canning, Thomas N.: Some Experiments at High Supersonic Speeds on the Aerodynamic and Boundary-Layer Transition Characteristics of High-Drag Bodies of Revolution. NACA RM A56I05, 1957.

8. Fisher, Lewis R.: Equations and Charts for Determining the Hypersonic Stability Derivatives of Combinations of Cone Frustums Computed by Newtonian Impact Theory. NASA TN D-149, 1959.

9. Seiff, Alvin, and Wilkins, Max E.: Experimental Investigation of a Hypersonic Glider Configuration at a Mach Number of 6 and at Full-Scale Reynolds Numbers. NASA TN D-341, 1961.

TABLE I.- TEST CONDITIONS AND DATA

Run no.	V, fps	M	R, million	ρ, slug/ft^3	d, in.	$\frac{x_{cg}}{d}$	I, slug-ft^2	σ_m, deg	σ_o, deg	$\sqrt{\overline{\sigma^2}}$, deg	λ, ft	$C_{m_{\sigma_L}}$, deg^{-1}	C_{N_α}, deg^{-1}	C_D
306R	5,790	5.14	0.216	0.000380	0.4463	0.766	1.212×10^{-7}	12.2	1.5	8.6	70.2	-0.00220	0.0165	0.590
908	10,020	14.4	3.56	.001536	.4511	.782	1.296	---	---	12.7	---	---	---	.574
909	9,670	14.2	3.58	.001549	.4500	.808	1.269	---	---	17.3	---	---	---	.623
943	11,500	17.2	4.01	.001566	.4020	.705	$.7063\times10^{-7}$	23.9	6.0	17.4	18.9	-.00590	---	.700
944	10,960	16.3	3.68	.001525	.4025	.712	.7040	23.0	5.0	16.7	18.6	-.00620	---	.666
945	10,810	16.1	3.44	.001447	.4011	.700	.6819	35.8	5.0	25.7	17.9	-.00693	---	.831
946	10,740	16.0	3.40	.001437	.4016	.701	.6797	39.9	.8	28.2	18.1	-.00679	---	.881
957	11,900	17.6	2.40	.000921	.4009	.710	.740	11.7	1.4	7.1	39.2	-.00246	.013	.584
960	11,490	16.8	2.19	.000897	.4011	.701	.7378	24.3	.8	17.3	25.0	-.00620	---	.665
962	11,800	17.4	2.33	.000912	.4015	.704	.7428	10.45	1.0	7.3	42.4	-.00213	.012	.577

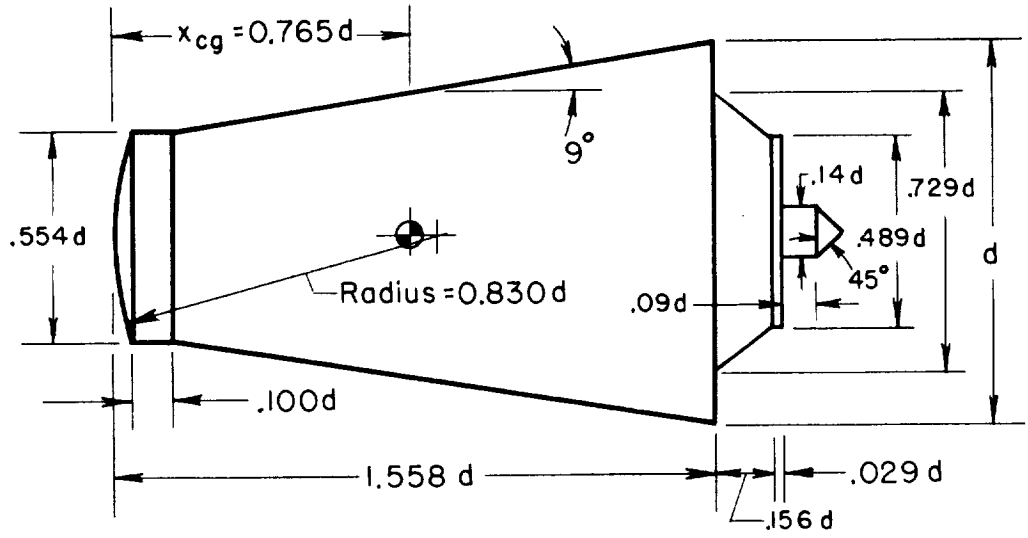

(a) Design center of gravity.

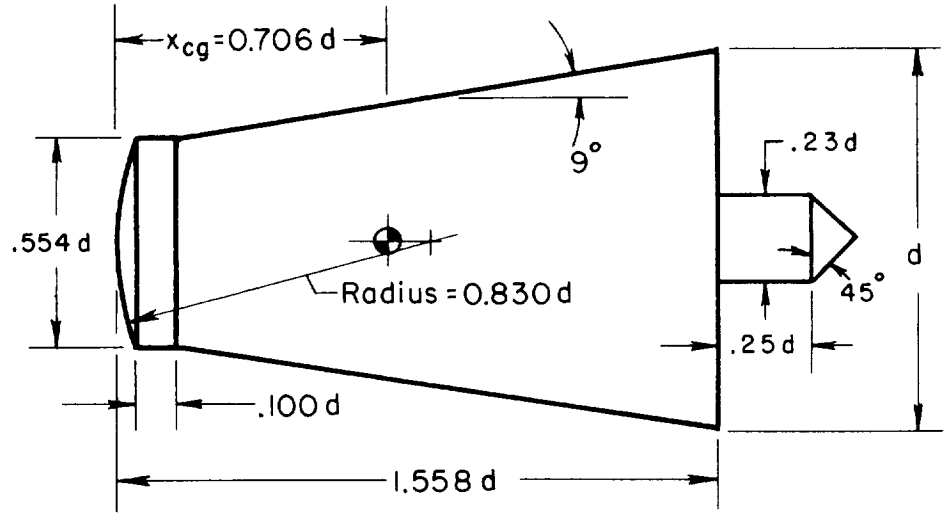

(b) Forward center of gravity.

Figure 1.- Test configurations.

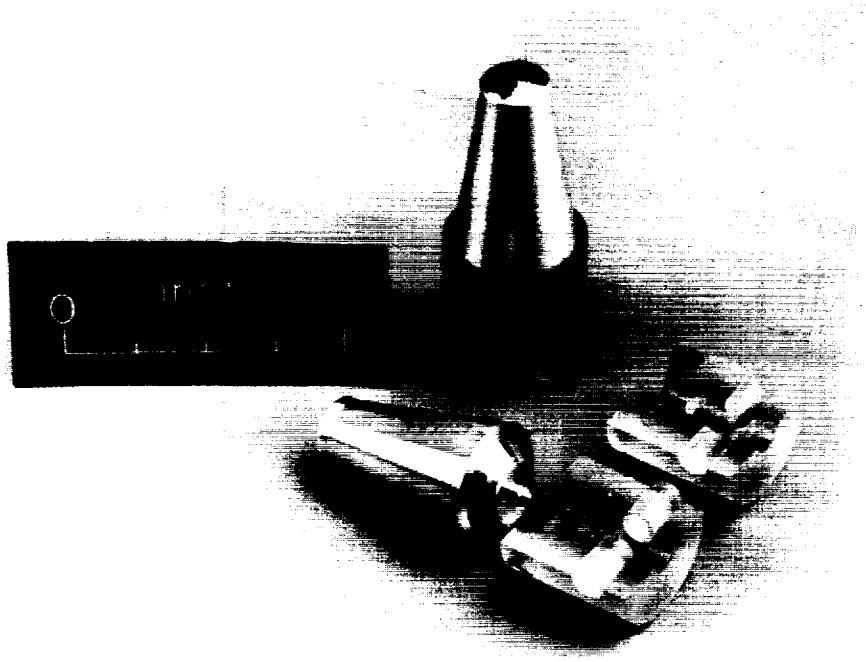

(a) Design center of gravity. A-27895

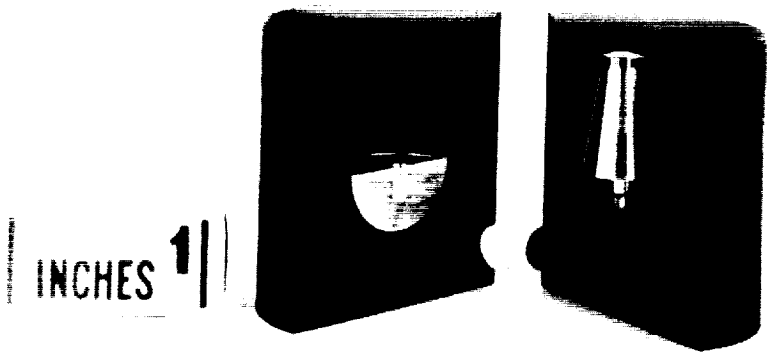

(b) Forward center of gravity. A-29206

Figure 2.- Photographs of models and sabots.

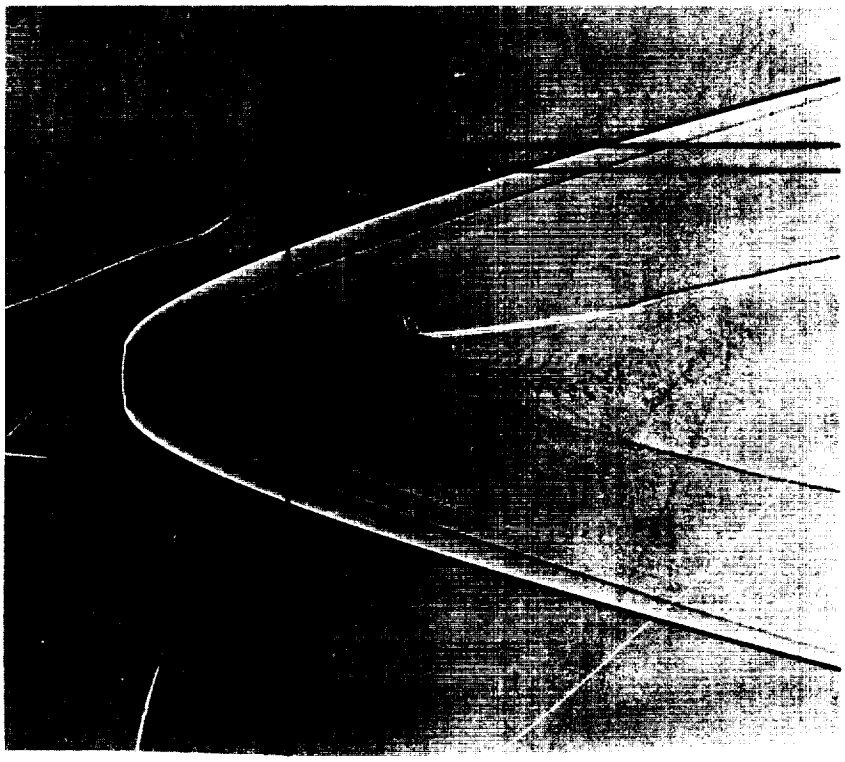

(a) Design center of gravity, M = 5.1. A-28022

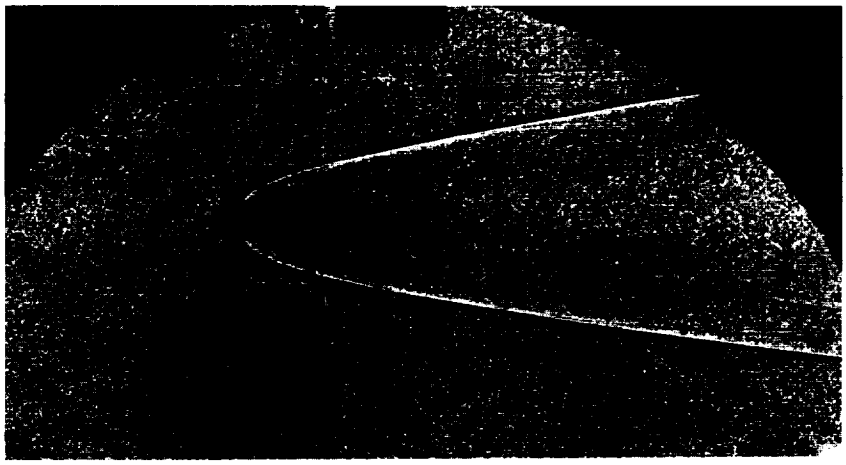

(b) Forward center of gravity, M = 17.4.

Figure 3.- Shadowgraphs of models in flight.

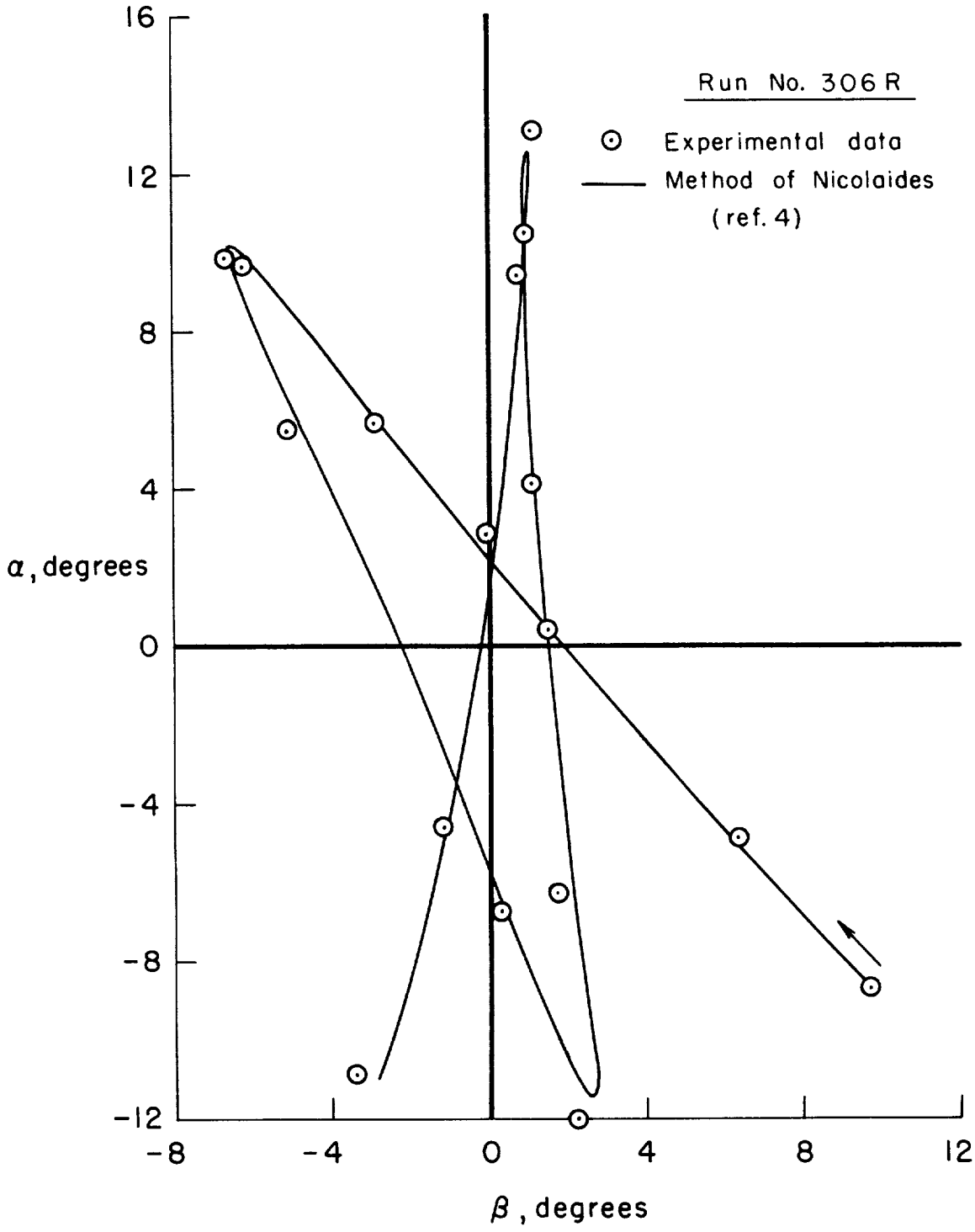

(a) Design center of gravity, M = 5.1.

Figure 4.- Typical pitching and yawing motions.

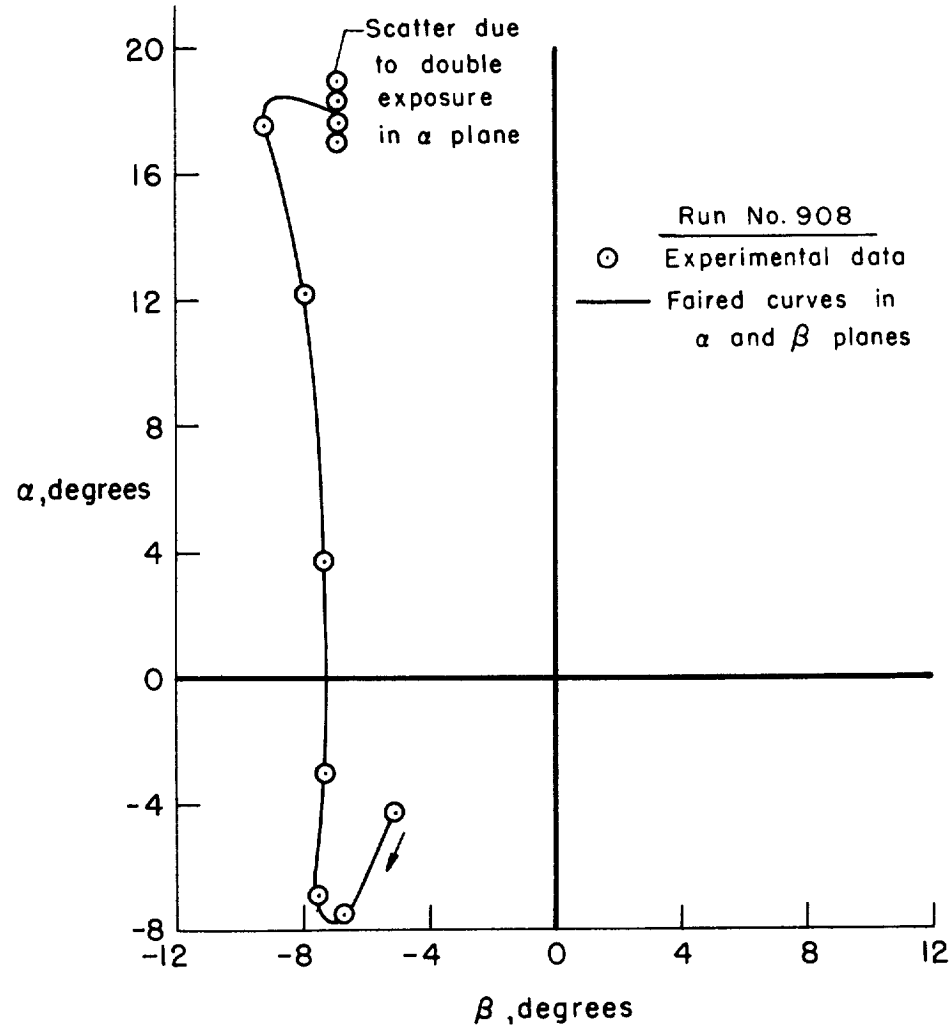

(b) Design center of gravity, M = 14.4.

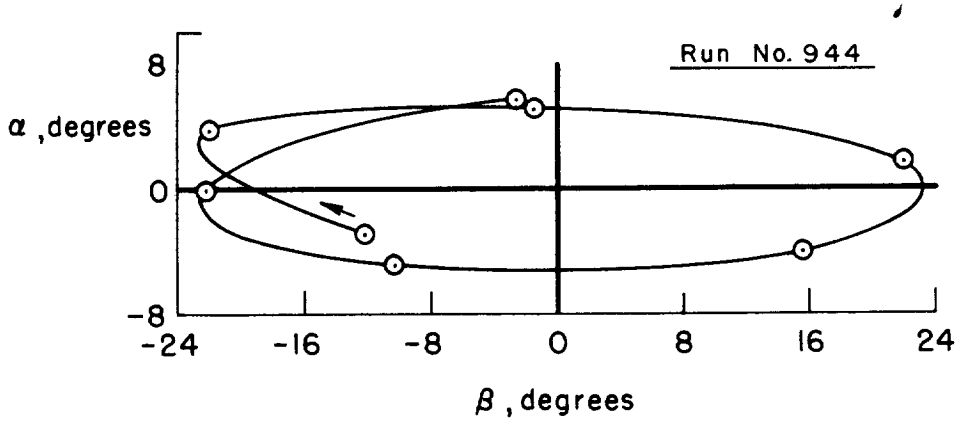

(c) Forward center of gravity, M = 16.3.

Figure 4.- Concluded.

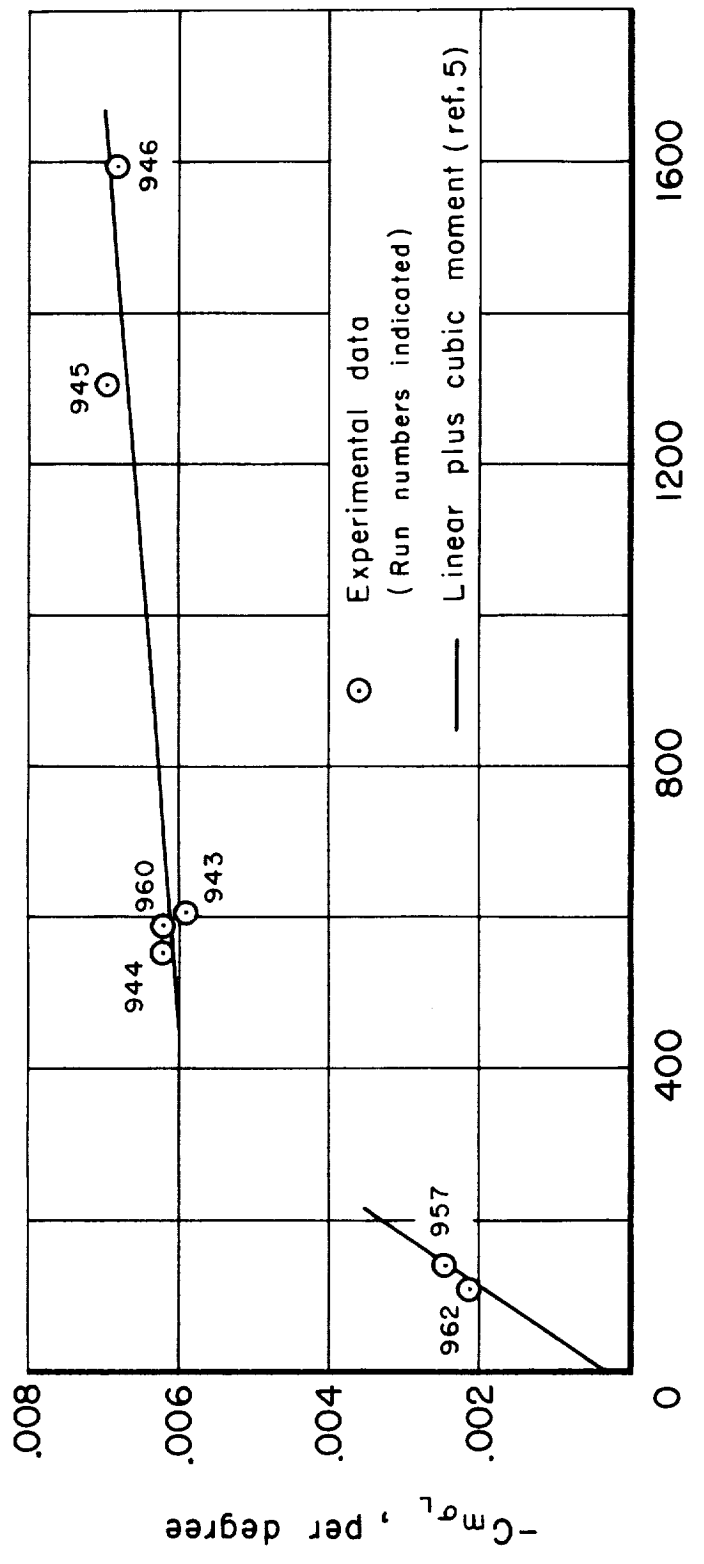

Figure 5.- Moment-curve slope from linear theory as a function of resultant angle of attack parameter.

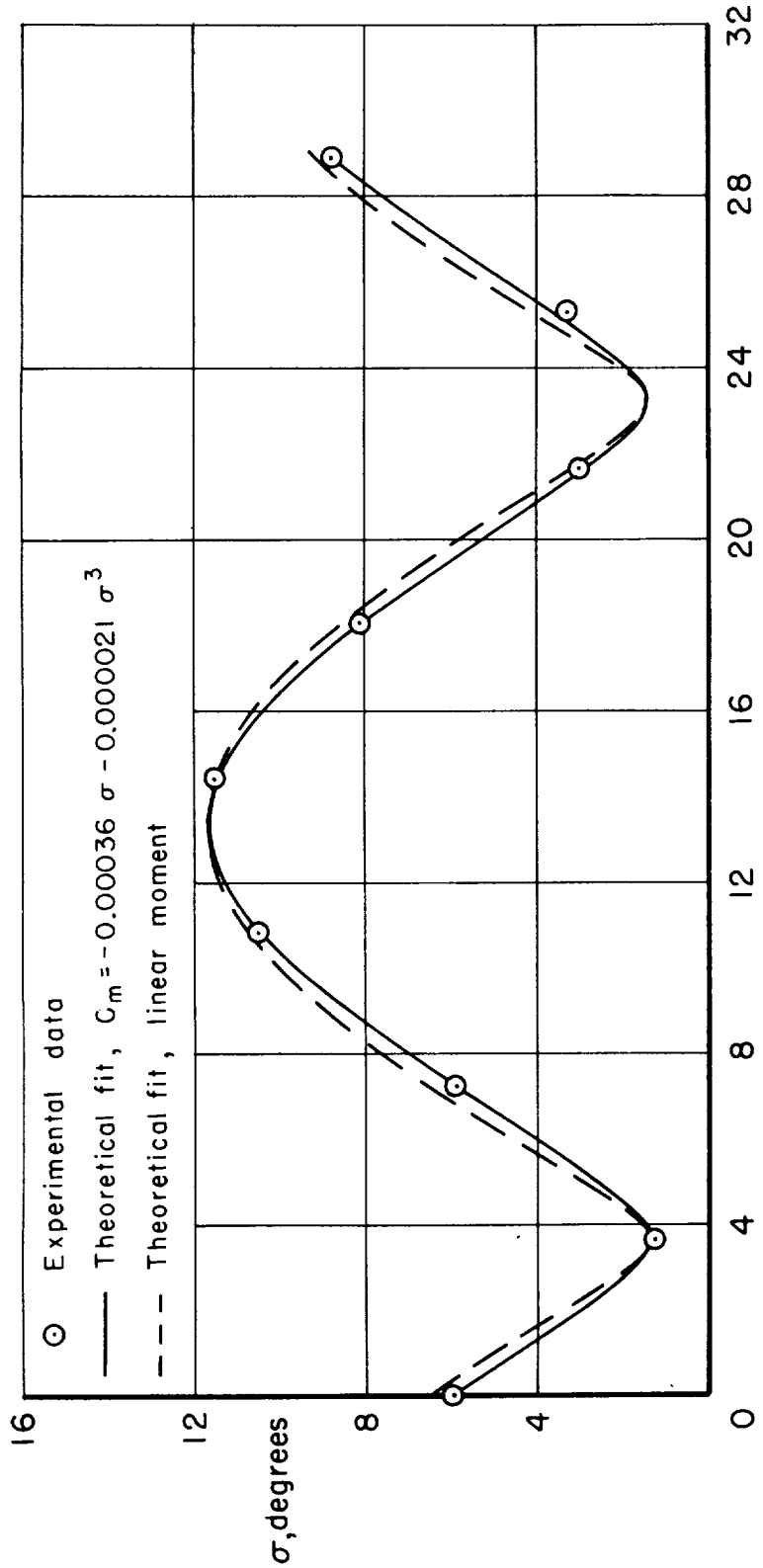

(a) Run 957, M = 17.6.

Figure 6.- Resultant angle of attack variation.

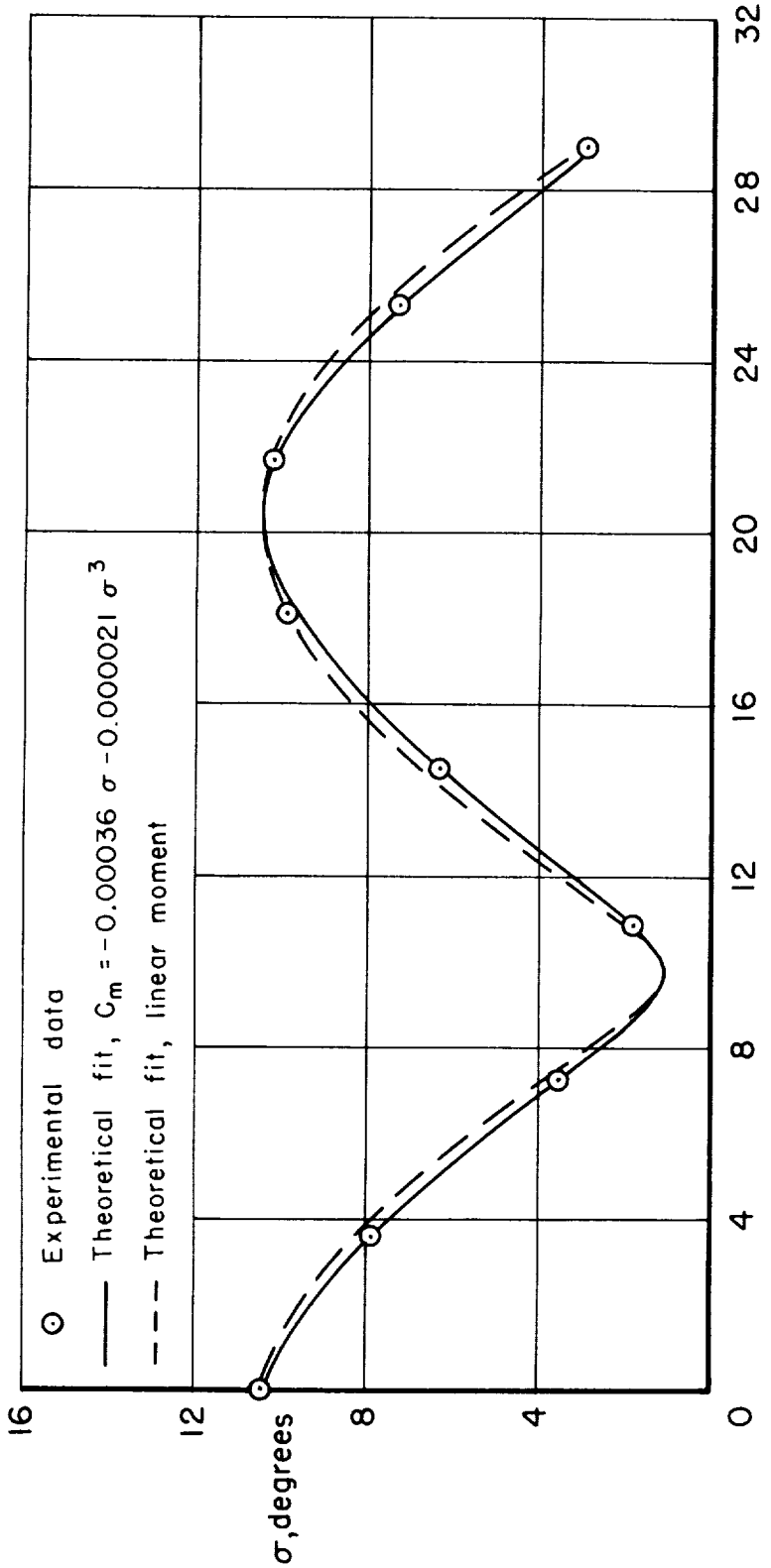

(b) Run 962, M = 17.4.

Figure 6.- Concluded.

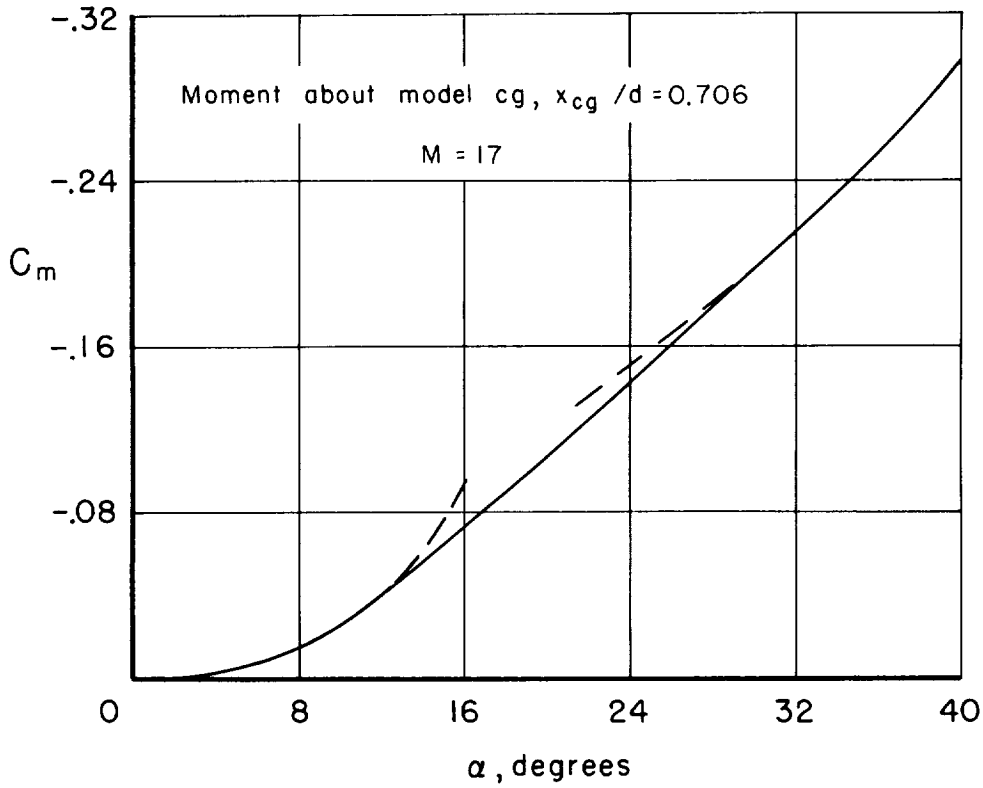

(a) Results of linear plus cubic moment assumption.

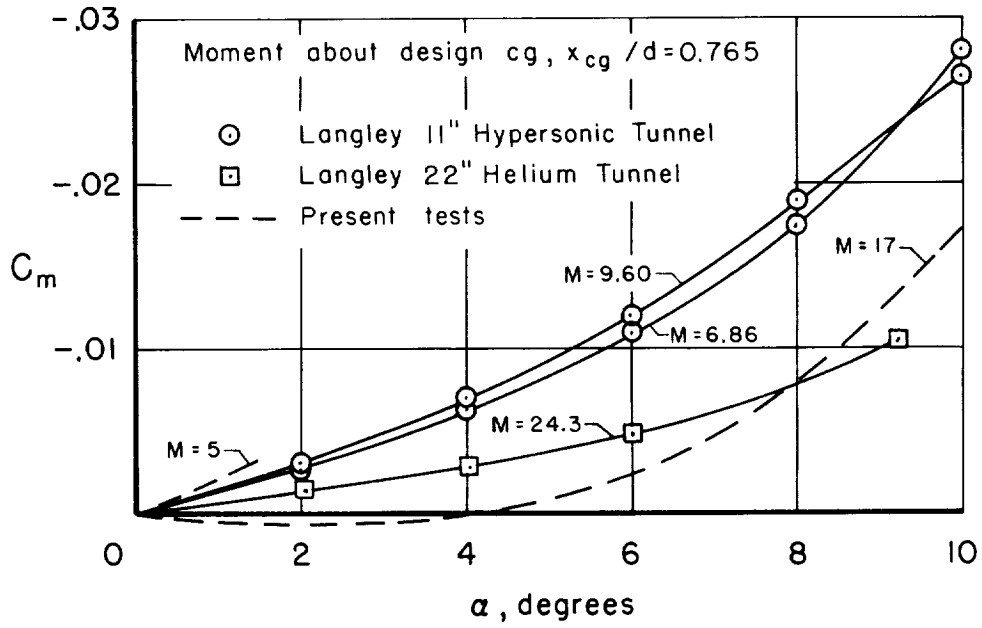

(b) Comparison with wind-tunnel data.

Figure 7.- Restoring moment coefficient.

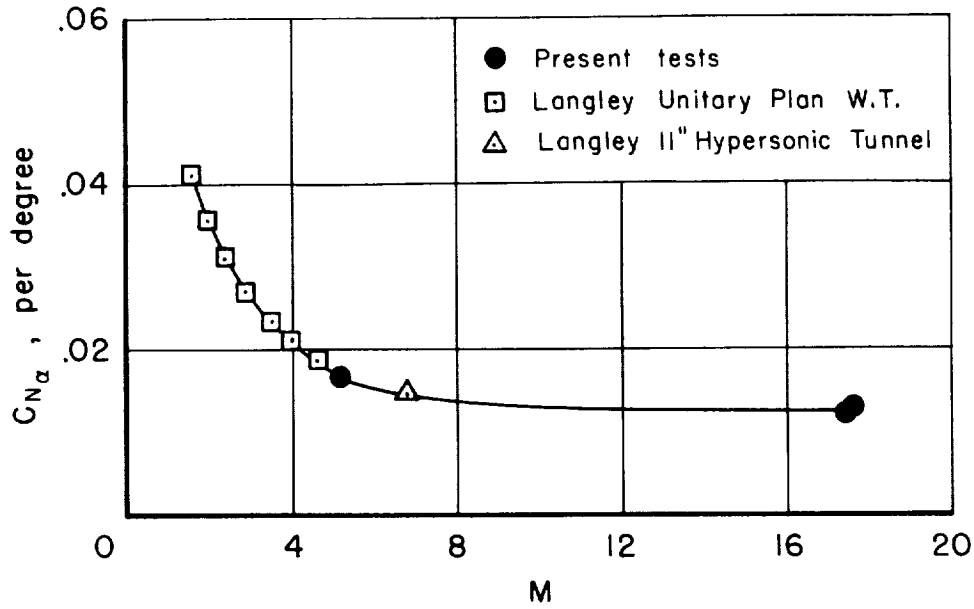

(a) Normal-force-curve slope as a function of Mach number.

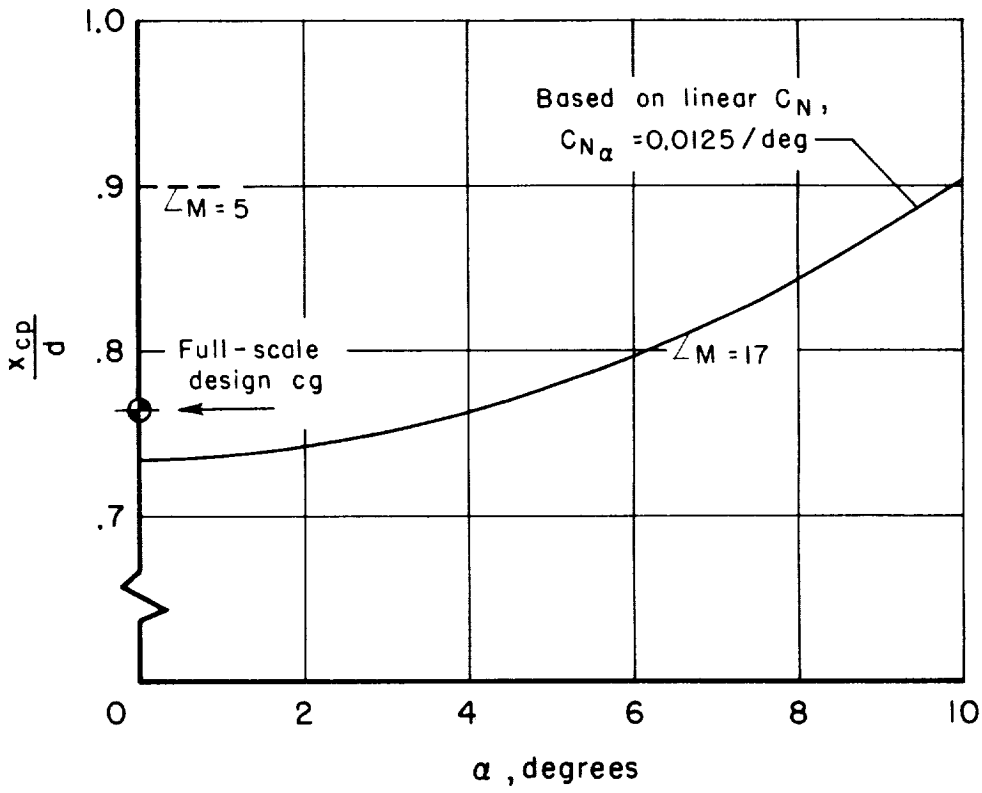

(b) Center of pressure as a function of angle of attack.

Figure 8.- Normal force and center of pressure.

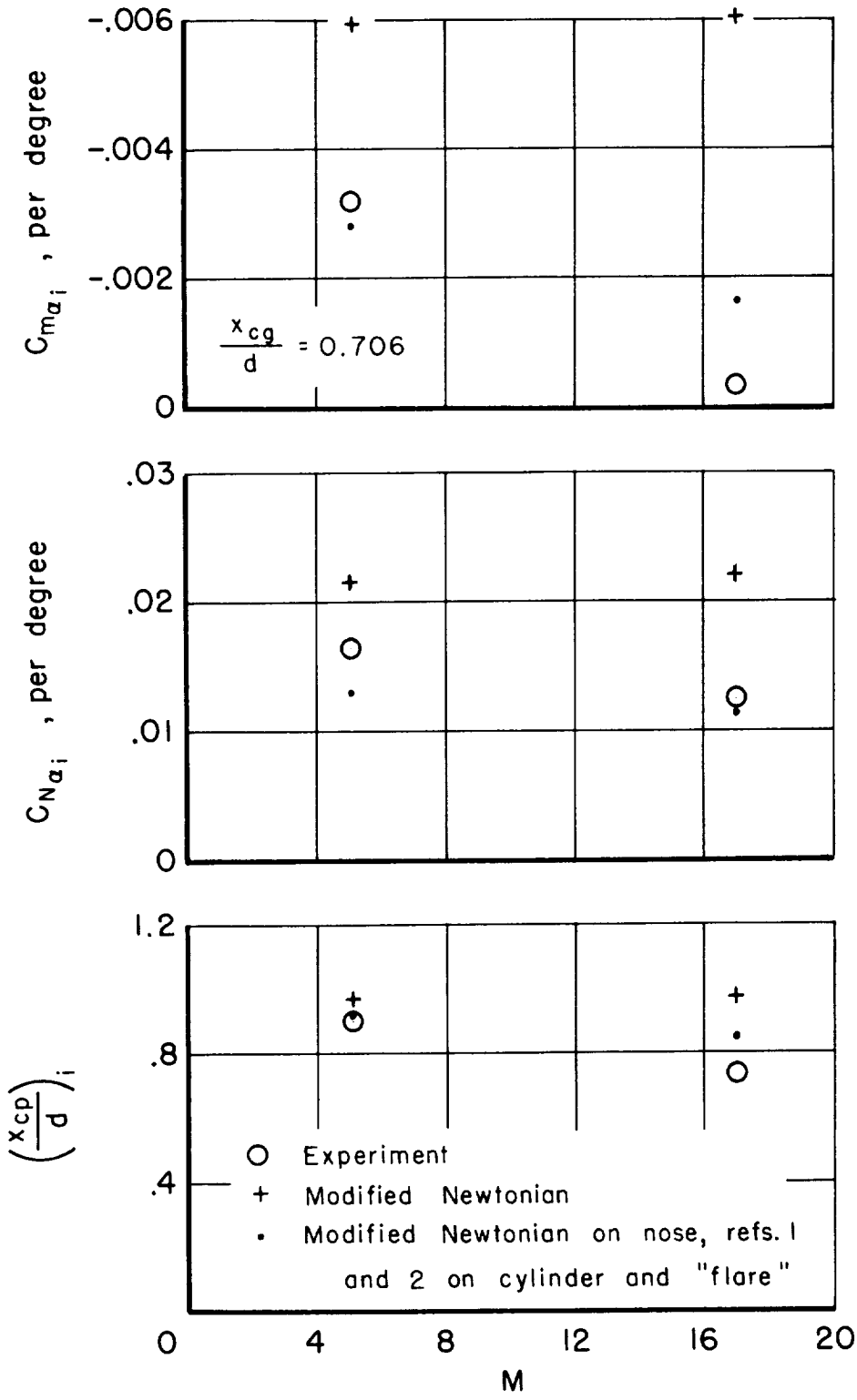

Figure 9.- Comparison with theory.

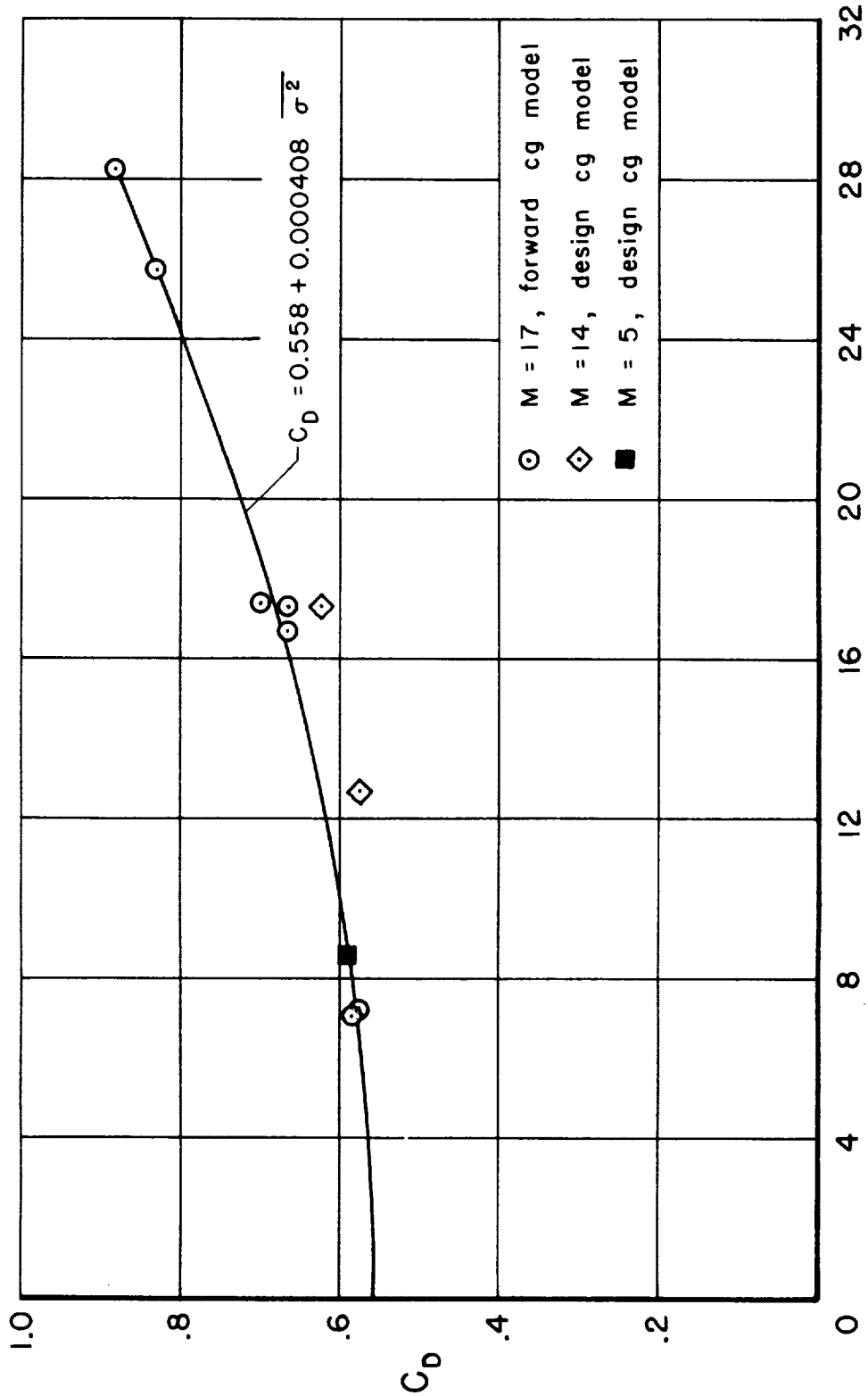

Figure 10.- Drag coefficient.

NASA-Langley, 1962 A-666